CHAPTER 202

LONGSHORE CURRENT AND LATERAL MIXING IN THE SURF ZONE

Ichiro Deguchi[1], Toru Sawaragi[2] and Masanobu Ono[3]

Abstract

We investigated the occurrence of FIG waves generated by a shear instability of steady longshore current on a uniformly sloping beach so that we can discuss the characteristic of Fig waves with respect to a wave breaking. We also carried out experiment to investigate cross-shore distribution of lateral mixing coefficient that determines the cross-shore profile of longshore current.

It is found that the occurrence and characteristic of FIG waves depend on a cross-shore profile of steady longshore current on the uniformly sloping beach as well as those on a beach of a constant depth analyzed by Bowen et al.(1989). The bottom slope affects FIG waves indirectly through the cross-shore profile of longshore current. The measured lateral mixing coefficient, which also gives influence on longshore currents, becomes maximum within the surf zone and decreases rapidly toward offshore. The locus where the maximum longshore current occurs, that plays an important role in the generation of FIG waves, depends on the surf similarity parameter of the incident wave.

Introduction

Various research regarding long period waves in a coastal region have been carried out. An object of the most of research is a long period wave corresponding to infragravity band. Wave number k_i of a long period wave of infragravity band is in a range of $\sigma^2/g<k_i<\sigma^2/(g\tan\beta)$ and does not become larger than $\sigma^2/(g\tan\beta)$, where σ is the angular frequency, g is the gravitational acceleration and $\tan\beta$ is the bottom slope.

According to recent field studies, waves of large wave numbers (short wave lengths) were observed in the lower frequency band than the infragravity band. Bowen et al.(1989) named such wave far infragravity wave (FIG wave). They analyzed the occurrence and characteristic of FIG waves and reported that a shear instability of steady longshore current caused FIG waves. However, their analysis was carried out

[1] Assoc. Prof., [2] Prof. and [3] Research. Assoc., Dept. of Civil Eng., Osaka University, Yamada-oka, Suita-city, Osaka 565, Japan

under the simplified condition where a constant water depth and a linear distribution of longshore current were assumed.

We analyzed the occurrence of FIG wave caused by the shear instability of steady longshore current on a uniformly sloping beach, a more realistic condition. We also examined the characteristic of lateral mixing coefficient that determines the cross-shore distribution of longshore current and accordingly exerts an influence on the occurrence of FIG wave greatly.

Occurrence condition of FIG wave on a uniformly sloping beach

In this section, we analyze the characteristic of FIG wave under the condition where a steady longshore current develops on a long straight beach with parallel contours. A coordinate system is shown in Fig.1. An x axis is taken positive in the offshore direction from the still water shoreline and a y axis in the longshore direction.

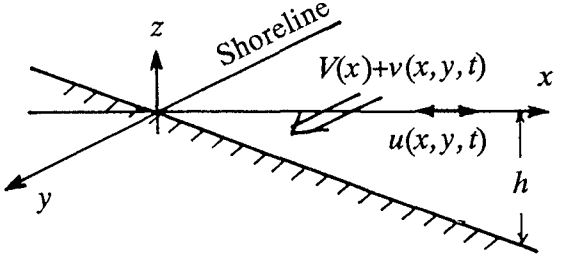

Figure 1 Coordinate system

We assume that a perturbed motion is superimposed on the steady longshore current. Let cross-shore and longshore components of perturbed velocity be $u(x,y,t)$ and $v(x,y,t)$ and the depth averaged velocity of steady longshore current be $V(x)$ where $V>>(u \text{ and } v)$. We also express the surface displacements corresponding to the perturbed motion and a steady component as $\eta(x,y,t)$ and $E(x)$.

The following fundamental equations for the steady component and perturbed component are obtained from a basic equation of a wave-induced current.

$$0 = -\frac{\partial E}{\partial x} - \frac{1}{\rho D}\frac{\partial S_{xx}}{\partial x} \tag{1}$$

$$0 = -\frac{1}{\rho D}\left(\frac{\partial S_{xy}}{\partial x} + \tau_y\right) + K_{xy}\frac{\partial^2 V}{\partial x^2} \tag{2}$$

$$\frac{\partial u}{\partial t} + V\frac{\partial V}{\partial y} = -g\frac{\partial \eta}{\partial x} \tag{3}$$

$$\frac{\partial v}{\partial t} + u\frac{\partial V}{\partial x} + V\frac{\partial v}{\partial y} = -g\frac{\partial \eta}{\partial y} \tag{4}$$

where ρ is the density of water, τ_y is the time averaged bottom shear stress in the longshore direction, S_{xx} and S_{xy} are the radiation stresses, K_{xy} is the lateral mixing coefficient and D is the total water depth $(=h+E+\eta)$.

We also suppose that a temporal variation of D is sufficiently smaller than spatial gradients of horizontal mass flux(uD and vD) of perturbed motion in cross-shore and

longshore directions. The following equation of continuity for perturbed motion is obtained.

$$\frac{\partial uD}{\partial x}+\frac{\partial vD}{\partial y}=0 \qquad (5)$$

We define a transfer stream function Ψ by Eq.(6) that has a form of Eq.(7):

$$uD=-\frac{\partial \Psi}{\partial y},\quad vD=\frac{\partial \Psi}{\partial x} \qquad (6)$$

$$\Psi=\mathrm{Re}\{\phi(x)\exp[i(ky-\sigma t)]\} \qquad (7)$$

where Re{ } expresses a real part of the complex quantity inside { }, σ and k are the angular frequency and the wave length of perturbed motion.

Eliminating η from Eqs.(3) and (4) and replacing (u, v) with Ψ by using Eq.(6), the following equation regarding $\phi(x)$ is obtained.

$$(V-\sigma/k)\{\phi_{xx}-k^2\phi-(D_x/D)\phi_x\}-\phi D(V_x/D)_x=0 \qquad (8)$$

where subscript x indicates a partial differentiation regarding x. The term V_x/D indicates the background potential vortex.

Bowen et al.(1989) supposed a triangular distribution of longshore current on a beach of constant water depth. Under such assumption, D_x in Eq.(8) becomes 0. They solved Eq.(9) and discussed the characteristic of FIG waves based on the solution that is expressed by a hyperbolic function.

$$\phi_{xx}-k^2\phi=0 \qquad (9)$$

However, there exists a bottom slope actually. Incident waves do break on the sloping bottom and longshore current generates. We examined various bottom profile where an analytical solution to Eq.(10) is obtained under the condition of $(V_x/D)_x=0$ in Eq.(8).

$$\phi_{xx}-k^2\phi-(Dx/D)\phi_x=0 \qquad (10)$$

It is found that when the bottom profile is expressed by Eq.(11), Eq.(10) becomes a modified Bessel's differential equation, Eq.(12).

$$D=x\tan\beta \qquad (11)$$

$$\phi_{xx}-(1/x)\phi_x-k^2\phi=0 \qquad (12)$$

A general solution to Eq.(10) is given by the first order modified Bessel functions of 1st and 2nd kind, I_1 and K_1 as follows:

$$\phi=pI_1(kx)+qK_1(kx) \qquad (13)$$

where p and q are the integral constant. On the other hand, the surface displacement of perturbed motion is calculated by eliminating u, v from Eq.(4) by using Eqs.(6) and (7) as follows:

$$\eta=-\{(V-\sigma/k)\phi_x-V_x\phi\}/gD \qquad (14)$$

We assume the same profile of V_x/D as Bowen et al. did. According to this assumption, a distribution of longshore current becomes the full line shown in Fig.2. A notation X_0 is the width of the longshore current whose velocity becomes the maximum ($V=V_0$) at $x=\delta X_0$ ($0<\delta<1$). In the figure, the bottom profile and the distribution of longshore current assumed in the analysis of Bowen et al.(1989) are shown by broken lines.

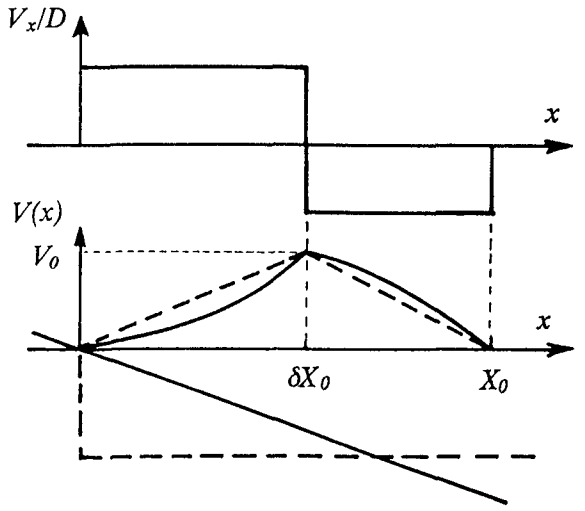

Fig.2 Cross-shore distributions of V_x/D and $V(x)$

The boundary conditions that the solutions in the regions of $0 \le x \le \delta X_0$ *and* $\delta X_0 \le x \le \infty$ have to satisfy are given as follows:

$\phi(x)=0$: at $x=0$ and $x=\infty$, and

Continuities of ϕ and η : at $x=\delta X_0$

When we eliminate integral constants in Eq.(13) by using these boundary conditions, the following dispersion relation for the perturbed motion is obtained:

$$a\sigma'^2+b\sigma'+c=0 \qquad (15)$$

$$a = F_1F_d \quad , \quad b = F_d/(1-\lambda)-F_1(k' F_d-\lambda)$$

$$c = \{1/(\delta-1)\}\left[\lambda\{1-(I_{1d}/I_{11})(K_1/K_{1d})\}-k' F_d\right]$$

$$\lambda = 1/\delta+1/(1-\delta) \quad ,$$

$$F_1 = (I_{01}+I_{21})/(2I_{11})+(K_{01}+K_{21})/2K_{11},$$

$$F_d = (I_{0d}+I_{2d})/(2I_{1d})+(K_{0d}+K_{2d})/2K_{1d},$$

$$K_{jd} = K_j(k'\delta) \quad , K_{j1} = K_j(k'), \; I_{jd} = I_j(k'\delta) \quad , I_{j1} = I_j(k'),$$

where, $\sigma'(=\sigma/(V_0/X_0))$ is the non-dimensional angular frequency, $k'(=kX_0)$ is the non-dimensional wave number, I_j and K_j $(j=0,1,2)$ are the j-th order modified Bessel function of 1st and 2nd kinds.

From, Eq.(15), it is found that when σ' becomes a complex $(\sigma'=\sigma_r'+i\sigma_i')$ with the negative imaginary part$(\sigma_i'<0)$, the perturbed motion becomes unstable and the amplitude of perturbed motion increases exponentially with time. FIG waves are generated by this instability and σ_i' becomes a growth rate of FIG wave. This instability occurs under the following condition.

$$b^2-4ac<0 \qquad (16)$$

We can also see that the non-dimensional angular frequency is a function of non-dimensional wave number k' and δ that is a parameter indicating the relative location where the maximum longshore current occurs. The bottom slope has noting to do with the angular frequency explicitly.

Figure 3 shows the relation between k' and σ_r' calculated from Eq.(15). In the figure, the region where Fig waves can occur is also illustrated. Figure 4 is the relation between σ_i' and k' when Eq.(15) has complex solutions.

As the value of δ increases the region where FIG wave occur spreads to the high waves number. The growth rate of FIG wave also becomes large. According to the results obtained by Bowen et al.(1989) both upper and lower limits in the wave number for the presence of FIG waves exist. However, only the upper limit in the wave number exists on the sloping beach.

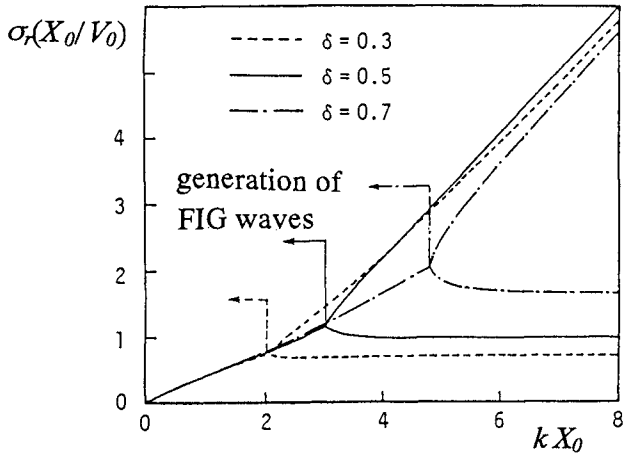

Fig.3 Relation between non-dimensional angular frequency and non-dimensional wave number and occurrence range of FIG waves.

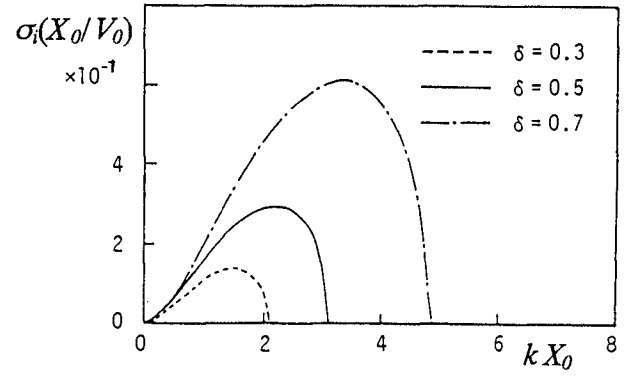

Fig.4 Growth rate of FIG wave

Figure 5 shows a relation between δ and the maximum nondimensional wave number k'_m of FIG wave.

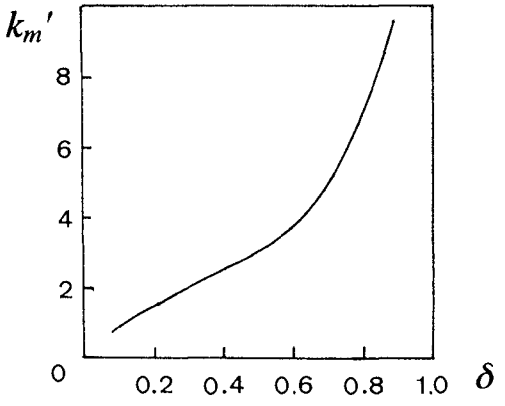

Fig.5 The maximum nondimensional wave number of FIG wave

Figure 6 shows the change of nondimensional celerity C_p' of FIG wave defined by $\sigma_r'/k'(=(\sigma/k)/V_0)$ with the non-dimensional wave number k' *in* the cases of δ=0.3, 0.5 and 0.7. The values of C_p' of different values of δ in Fig.6 do not show any significant difference.

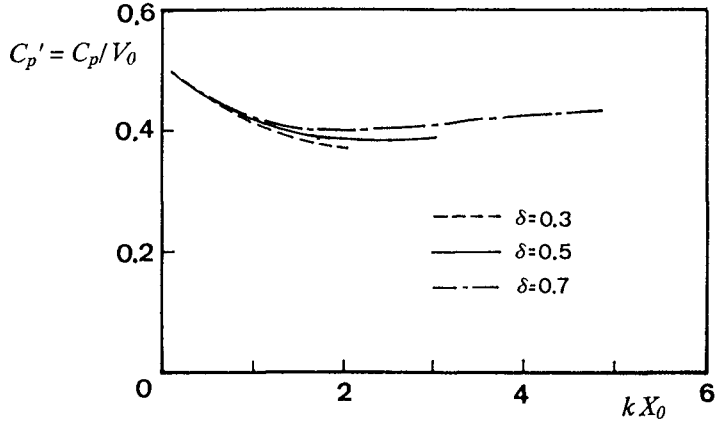

Fig.6 Nondimensional celerity of FIG wave

From these results, it is found that the occurrence of FIG wave depends on only the value of δ and the wave number and the angular frequency of FIG wave are determined by the values of X_0, δ and V_0. Also, the wave number of FIG wave is sufficiently larger than those of long waves of leaky mode($<\sigma^2/g$) and of edge

wave($<\sigma^2/(g\tan\beta)$). For instance, when V_0=1m/s, X_0=20 m, $\tan\beta$=0.1 and δ=0.5, FIG wave exists in the region of k<0.15 and σ<0.058 from Fig.3. The wave period and the wave length corresponding to the maximum angular frequency are 108s and 41.9 m, respectively.

Cross-shore distribution of longshore current velocity

As mentioned above, the characteristic of FIG wave deeply depends on a cross-shore distribution of steady longshore current. Many studies have been carried out about the steady longshore current on the long straight beach based on Eqs.(1) and (2). For example, an analytical solution of the velocity of steady longshore current derived by Longuet-Higgins (1970) is expressed as follows:

$$V/V_b = A(x/x_b) + B_1(x/x_b)^r \quad for \quad x/x_b \le 1 \tag{17}$$
$$V/V_b = B2(x/x_b)^s \quad for \quad x/x_b > 1$$

$$V_b = \frac{5\pi}{16}\frac{\tan\beta}{C_f}\sqrt{gD_b}\sin\theta_b \tag{18}$$

$$p = \pi N\tan\beta/(\gamma C_f) \ , \quad A = 1/(1-5p/2) \ ,$$
$$r = \left\{-3/4 + \sqrt{9/16+1/p}\right\} \ , \quad s = \left\{-3/4 - \sqrt{9/16+1/p}\right\} \ , \tag{19}$$
$$B_1 = A(s-1)/(r-s) \ , \quad B_2 = A(r-1)/(r-s) \ ,$$

where N in the expression of p is the constant relating to a lateral mixing coefficient, γ is the ratio of wave height to water depth, C_f is the friction factor and subscript b indicates the value at the wave breaking point.

As can be seen from Eqs.(17) and (18), the distribution and the absolute value of the longshore current velocity are determined by the values of p and V_b. Furthermore, V_b is decided by the celerity C_b, the wave direction θ_b and γ_b at the wave breaking point if the assumption of $\tan\beta/C_f$=constant (Komar, 1976) is correct. The value of p also depends on only N and γ.

The point where the longshore current becomes maximum ($x=\delta X_0$) and the maximum velocity of longshore current ($V=V_0$) are determined by differentiating Eq.(17) with respect to x. However, we are not able to decide the width X_0 of the longshore current easily. We must newly define the width of the longshore current by some methods, to evaluate the value of X_0. Here, we approximated the width X_0 by the width of breaker zone x_b.

Figure 7 shows the relation between the maximum longshore current velocity and the relative location where the velocity of longshore current becomes the maximum to the breaker zone defined by $\delta'(=\delta X_0/x_b)$.

When we assume that the orders of $\tan\beta/C_f$ and γ are 10 and 1, respectively, the value of p becomes about $p=30N$ from Eq.(19). At this time, the value of p changes in a range of $0.03<p<0.9$ with the range of N=0.001 to 0.03. According to these, the value of δ' changes between 0.7 and 0.4 from Fig.7. However, the value of $\tan\beta/C_f$ is not always constant in fact. Even γ changes with the bottom slope and the incident wave characteristic. Therefore, we examine the distribution of longshore current velocity and the value of N from experimental results.

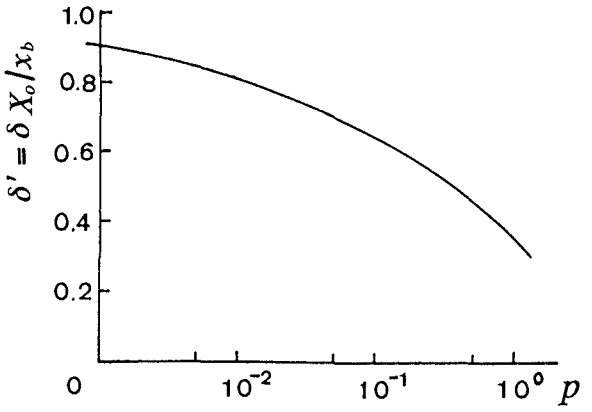

Fig.7 Locus where the maximum velocity of longshore current occurs

Experiment on velocity distribution of longshore current and lateral mixing coefficient

(1) Method of experiments and experimental conditions

Some experimental researches have already carried out about the distribution of longshore current. The steady longshore current on a long straight beach of uniform sloping beach is determined from the balance of driving force expressed by the gradient of the radiation stress, the bottom shear stress and the gradient of time and depth averaged Reyneods' stress. This relation is indicated by Eq.(2) and the solution to that is given by , for example, Eq.(17).

Among these, the time and depth averaged Reynolds' stress is usually expressed by the lateral mixing term of diffusion type using lateral mixing coefficient K_{xy}. However, it is extremely difficult to measure the coefficient, directly. Accordingly, only a few discussions have reported about the lateral mixing coefficient based on the analogy of measured diffusion coefficient ε_{xy} in the surf zone under limited experimental conditions (for example Kim et al.(1982)). We carried experiments in a wave basin to measure longshore current and diffusion coefficient under a wide range of a surf similarity parameter assuming that the lateral mixing coefficient has similar property to the diffusion coefficient. Based on the measured results, we examine the dependencies of longshore current and the value of p on the surf similarity parameter and the possibility of the occurrence of FIG waves in the wave basin.

However, the longshore current that occurs in the wave basin with the limited width receives an influence of side walls of the basin. As was already pointed out by Visser(1991), the longshore current in the wave basin is different from that calculated from Eq.(17). We also examine this point based on the experimental results.

The wave basin used in the experiment is 20m long, 10m wide, and 0.6m deep. A mortar coated model uniformly sloping model beach was made at the end of the wave basin. The angle on wave incidence was 30° to the contour of the beach at the depth of 40cm. Two kinds of bottom slopes of 1/10 and 1/20 were examined.

Figure 8 is the illustration of the outline of the experimental set-up and Table-1 shows the experimental condition.

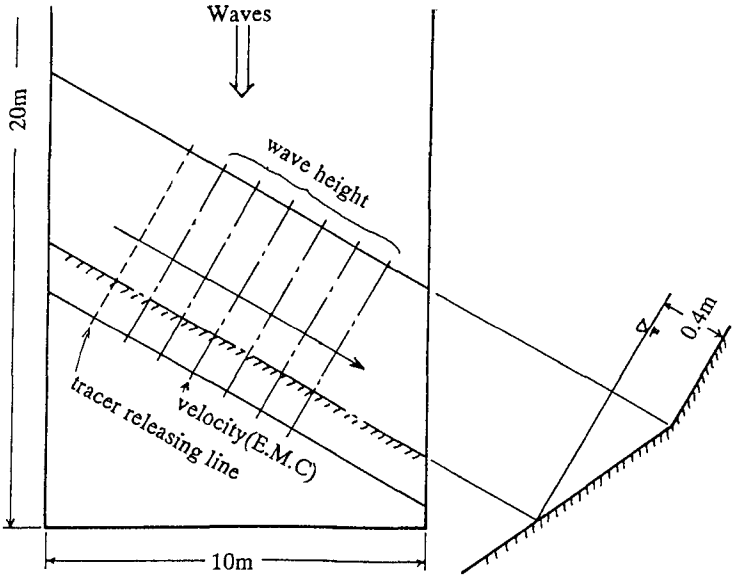

Fig.8 Experimental set-up

Table 1 Experimental condition

Case No.	H (cm)	T (s)	ξ	x_b (cm)	X_0 (cm)	V_0 (cm/s)	δ	δ'
4	10.9	1.0	0.38	170	180	70	0.40	0.42
5	10.3	1.2	0.47	160	170	72	0.47	0.50
6	10.2	1.4	0.55	140	170	75	0.47	0.57
7	7.6	1.0	0.23	210	210	35	0.33	0.33
8	7.0	1.2	0.28	200	220	37	0.38	0.40
9	7.0	1.4	0.33	170	190	40	0.42	0.47
10	10.4	1.0	0.19	270	270	45	0.37	0.37
11	9.5	1.2	0.24	250	260	50	0.38	0.40
12	9.3	1.4	0.29	230	260	44	0.42	0.49

Case 4-6 : $\tan\beta = 1/10$, Case 7-12 : $\tan\beta = 1/20$,

In the Table, ξ is a surf similarity parameter defined by $\tan\beta/\sqrt{H_0/L_0}$, where H_0 and L_0 are the equivalent wave height and length of incident waves in deep water.

We measured wave height along 5 measuring lines by capacitance type wave gauges at an interval of 10cm in the cross-shore direction. Vertical and cross-shore distributions of water particle velocity along the center measuring line were measured by an electromagnetic current meter. We also measured loci of tracers released at the same point to evaluate longshore current velocity as advection speed and diffusion coefficient by applying a so-called one particle analysis method.

The diffusion coefficient at $x=X_i$, $\varepsilon_{xy}(X_i)$, was evaluated using the following equation:

$$\varepsilon_{xy}(X_i)=\frac{1}{2}\frac{d\sigma_x(X_i,t)^2}{dt} \tag{20}$$

$$\sigma_x(X_i,t)^2=\sum_{j=1}^{j_e}\{X_i(j,t)-\overline{X_i}\}^2\Big/j_e \tag{21}$$

where j_e is a number of tracers, $\overline{X_i}$ is a mean cross-shore locus of at least 20 tracers whose initial released position is X_i and $X_i(j,t)$ ($j\geq 20$) is a position of j-th tracer after a time t released at X_i. The loci of tracers were measured by video analysis at time interval of 0.3s.

Results and discussion

(1) Lateral mixing coefficient

Various expressions for the lateral mixing coefficient have already proposed with respect to the steady longshore current on a long straight beach. When we normalize the lateral mixing coefficient by $x_b\sqrt{gD_b}$ or $\sqrt{gD_b}D_b/\tan\beta$, many of them can be expressed by the following form:

$$\varepsilon_{xy}'=\varepsilon_{xy}\Big/\left\{\sqrt{gD_b}\,D_b/\tan\beta\right\}=e(D/D_b)^n \tag{22}$$

Some examples of the expression e in Eq.(22) are shown in Table 2.

Table 2 Examples of expression for lateral mixing coefficient

	e	n
Longuet-Higgins(1970)	N (<0.01)	1.5
James(1974)	N :$D<D_b$ $N(D_b/D)^2$:$D_b<D$	1.5
Battjes(1975)	$M(5\gamma^2/16)^{1/3}\tan^{4/3}\beta$	1.5
Author et al.(1986)	$KF^{1/3}\gamma\tan\beta$:$D<D_b$ 0 :$D_b<D$ F=5.3-3.5ξ -0.07/tanβ	1.5

According to Longuet-Higgins(1970), e becomes a constant N. Battjes' expression implies that e is a function of $\tan\beta$ and γ. The author et al.(1982) also proposed that e is a function of $\tan\beta$, γ and ξ.

Figure 9 illustrates measured cross-shore distribution of non-dimensional diffusion coefficient $\varepsilon_{xy}'(=\varepsilon_{xy}/\sqrt{gD_b}D_b/\tan\beta)$. In the figure, a family of curves corresponds to the values of kxy' in the cases of e=0.00125,0.0025,.005 and 0.008 in Eq.(22). Numerals in the figure correspond to the case No. in Table 2.

It is found from the figure that measured diffusion coefficient does not show significant dependency on ξ. However, the values of ε_{xy}' in the cases of a steep slope beach ($\tan\beta$=1/10) are larger than those in the cases of a gentle slope beach ($\tan\beta$=

1/20). In the former cases the value of ε_{xy}' is in the region of 0.005-0.007 and 0.003-0.005 in the latter cases. It is also found that ε_{xy}' becomes maximum near D/D_b=0.7-0.8 and decreases rapidly toward offshore.

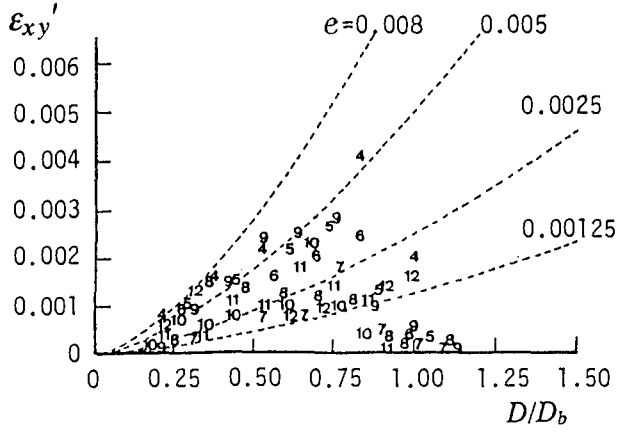

Fig.9 Cross-shore distribution of measured diffusion coefficient

(2) Cross-shore distribution of longshore current

Velocity of longshore current that was measured with an experiment differs from the velocity of longshore current in a seashore on a long straight line that is given with a solution of Eq.(2) due to an influence of a side wall of a reservoir.

Figure 10 show an example of comparison between calculated and measured longshore current velocity (Case-4). A solid line is the calculated result from the analytical solution on the long straight beach (Eq.(17)). Large open circles are the measured velocity by the electro-magnetic current meter and small circles are the advection speed of tracers. In the calculation of the velocity, we used the value of 0.005 for N in Eq.(17) according to the measured result. The value of friction factor was determined from the laminar boundary layer theory under waves and current.

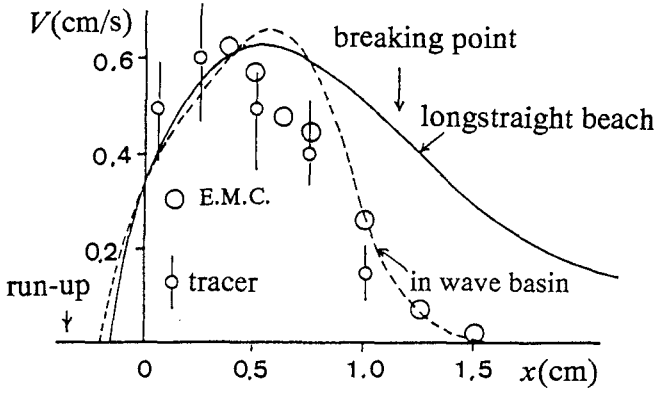

Fig. 10 Cross-shore distribution longshore current (Case-4)

The decrease of the measured velocity near the wave breaking point is faster than the calculated longshore current in the wave basin.

Figure 11 is the wave-induced current pattern obtained from the numerical simulation of wave and current fields in the wave basin.

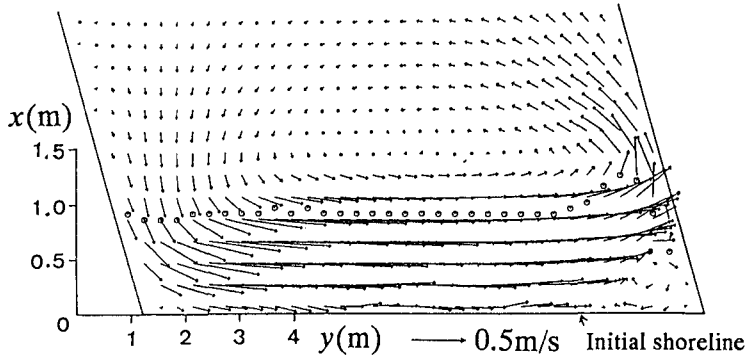

Fig.11 Simulated wave-induced current in the wave basin (Case-4)

It is found that the compensation flow generates outside the breaker zone. The broken line in Fig.10 is the cross-shore profile of longshore current in the center of the wave basin shown in Fig.11. The measure profile of longshore current is reproduced well by the simulated wave-induced current.

Although the measured longshore current in the deeper region around the breaking point is different from that of the analytical result on a long straight beach, the loci where the maximum longshore current occurs in both profiles differ a little. Therefore, we can discuss the relative location of δX_0 to the breaker width x_b ($=\delta'$) based on the experimental results.

Figure 12 shows the relation between δ' (δ) and the surf-similarity parameter ξ. The values of δ and δ' are shown in Table-1.

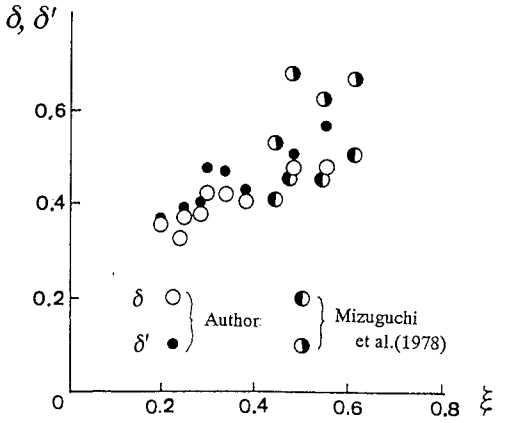

Fig.12 Relation between δ' (δ) and ξ

In the figure, experimental results of Mizuguchi et al.(1978) are shown. The value of δ' increases from 0.4 to 0.7 with the increase of ξ from 0.2 to 0.6. As I have already mentioned before, the change in the value of N corresponding to this change in δ' is from 0.001 to 0.03 that is a little larger than the measured change in the value of e. Therefore, It seems necessary to study the reason for this discrepancy together with the dependency of C_f and γ on the surf-similarity parameter.

In the experiment, we found the long period fluctuations in water surface displacement and horizontal velocity whose period was about 30s. The corresponding wave length of FIG wave is estimated to be about 6m from the dispersion relation that is about 1/2 of the length of shoreline in the wave basin.

Conclusions

We carried out the analysis of Fig waves on the unifromly sloping beach after the analytical investigation of Fig waves on a beach of constant depth by Bowen et al.. We also conducted experiments to examine the effect of lateral mixing on the cross-shore distribution of longshore current that determines the characteristic of FIG waves.

The main results obtained in this study are summarized as follows:

1. FIG waves on a uniformly sloping beach have upper limits in wave number and frequency.
2. The amplification factor (growth rate) of FIG wave becomes large as the locus where the maximum longshore current occurs becomes deep.
3. Measured diffusion coefficients show a little dependency on the surf-similarity parameter. They become maximum in the surf zone and decrease rapidly toward offshore.
4. The experimental results show that the locus where the maximum longshore current occurs becomes deep according to the increase of the surf-similarity parameter.

Reference

Battjes J.A., 1975, A note on modeling of turbulence in the surf zone, Proc. Symp. Modeling Technique, pp.1050-1061.

Bowen, A.J., and Holman, R.A., 1989, Shear instabilities of the mean longshore current (1. Theory), JGR, Vol.94, No.C12, pp.18023-18030.

James, I.D., 1974, A nonlinear theory of longshore current, Esturine and Coastal Marine Science, Vol.2, pp.207-234.

Kim, K.H., Sawaragi, T. and Deguchi, I.,1986, Lateral mixing and wave direction in the surf zone, Proc. 20th ICCE, pp.366-380.

Komar, P.D., 1976, Beach Processes and Sedimentation, Prentice Hall, pp.192-194.

Longuet-Higgins, M.S.,1970, Longshore currents generated by obliquely incident sea waves, JGR, Vol.75, No.C33, pp.6778-6789.

Mizuguchi, S., Ohshima Y. and Horikawa, K., 1978, Vertical distribution of longshore current, Proc. Japanese Conf. on Coastal Engineering, Vol.25, pp.425-429.(in Japanese)

Visser P.J.,1992, Laboratory measurements of uniform longshore currents, Coastal Engineering, 15, pp.563-593.